IOP Publishing Measurement Science and Technology
Meas. Sci. Technol. **23** (2012) 025005 (8pp) doi:10.1088/0957-0233/23/2/025005

Using a MEMS gyroscope to measure the Earth's rotation for gyrocompassing applications

L I Iozan[1], M Kirkko-Jaakkola[2], J Collin[2], J Takala[2] and C Rusu[1]

[1] Technical University of Cluj-Napoca, Baritiu 26-28, 400027 Cluj-Napoca, Romania
[2] Tampere University of Technology, PO Box 553, 33101 Tampere, Finland

E-mail: Lucian.Iozan@bel.utcluj.ro, martti.kirkko-jaakkola@tut.fi, jussi.collin@tut.fi, jarmo.takala@tut.fi and Corneliu.Rusu@bel.utcluj.ro

Received 16 May 2011, in final form 28 November 2011
Published 11 January 2012
Online at stacks.iop.org/MST/23/025005

Abstract
In this paper, a method and system for gyrocompassing based on a low-cost micro-electro-mechanical (MEMS) gyroscope are described. The proposed setup is based on the choice of a gyroscope with specified bias instability better than 2 deg h^{-1} and on careful error compensation. The gyroscope is aligned parallel to the local level, which helps to eliminate the *g*-sensitivity effect but also sacrifices a fraction of the Earth's rotation rate that can be observed. The additive bias is compensated for by rotating the sensor mechanically and by extended Kalman filtering. In this paper, it is demonstrated that the proposed system is capable of observing the Earth's rotation, and the north finding results show that a two-sigma accuracy of 4.03° was attained at latitude 61°N. With current MEMS gyroscopes, the system requires hours of time to achieve this accuracy, but the results demonstrate the theoretical accuracy potential of these small self-contained, low-cost sensors.

Keywords: gyrocompass, MEMS gyroscope, bias compensation

1. Introduction

Accurate heading is a key factor in many location systems and is typically obtained by using digital magnetic compasses (DMCs). These are compact, low-cost instruments capable of achieving sub-degree heading accuracies [1]. However, the heading accuracy of DMCs can be very easily degraded by nearby ferrous materials or by electromagnetic interference. For these reasons, DMCs are not very reliable indoors. In contrast, inertial gyrocompasses are unaffected by such factors and capable of maintaining a high level of accuracy regardless of the environment [2, 3]. Gyrocompasses operate by observing the Earth's rotation rate. This requires highly accurate sensors, and only recently have micro-electro-mechanical system (MEMS) gyroscopes been considered accurate enough to measure it [4, 5]. The ability to measure such slow rotation using low-cost, low-power, small-size sensors is very interesting from both academic and application viewpoints.

In this paper, we discuss the most significant error sources that degrade the performance of MEMS gyroscope sensors and propose ways of compensating for them in the context of gyrocompassing. This is done in order to maximize the performance of these sensors, which are usually designed as electronically driven resonators, often manufactured from a single piece of quartz or silicon. Such gyroscopes operate in accordance with the dynamic theory, which states that when an angular rate is applied to a translating body, a Coriolis force is generated [2, 6]. The force is proportional to the applied angular rate and causes a displacement that can be measured capacitively in a silicon instrument or piezoelectrically in a quartz instrument. Theoretically, if the errors of such gyroscopes are properly modeled and compensated for, it is possible to measure very small angular rates, like the Earth's rotation rate. In practice, however, this requires averaging a long sequence of observations, and if the bias instability of the gyroscope is not good enough, the small angular rate will be buried under bias drift. Consequently, the sensor must be chosen carefully.

The direct measurement of the Earth's rotation rate has been performed using a MEMS gyroscope in [4], while [7–9] report progress in the development of high-accuracy MEMS gyroscopes with north seeking capabilities. In [4], the sensitive axis of the gyroscope was parallel to the Earth's rotation axis, and long-term measurements were carried out in order to compensate for external factors (e.g., gravity) from the measurement data; in [8, 9], the errors were eliminated by means of carouseling.

This paper proposes an approach where the sensitive axis of the gyroscope is always parallel to the Earth surface. There are two main reasons for this: first, when seeking north, we are interested in the horizontal direction; thus, by keeping the sensor aligned with the local level, we need only rotations around a single axis, which keeps the mechanics simple. Secondly, the horizontal plane is perpendicular to the gravity vector, which causes the effect of g-sensitivity to remain constant after each rotation; this way, it is more straightforward to eliminate. On the other hand, the component of the Earth's rate that can be detected by a leveled sensor depends on the latitude and is less than half of the true rate in our tests at latitude 61.449°N. Furthermore, we eliminate the additive bias by periodical mechanical changes in the sensor orientation (also known as two-point gyrocompassing [9]), and the north direction and required correction values are estimated using an extended Kalman filter (EKF).

The paper is organized as follows. In section 2, the theoretical background including the EKF model and an analysis of the attainable accuracy is presented. The measurement setup is described in section 3, whereas section 4 demonstrates the theoretical and practical north finding capability of the proposed system. Section 5 concludes the paper.

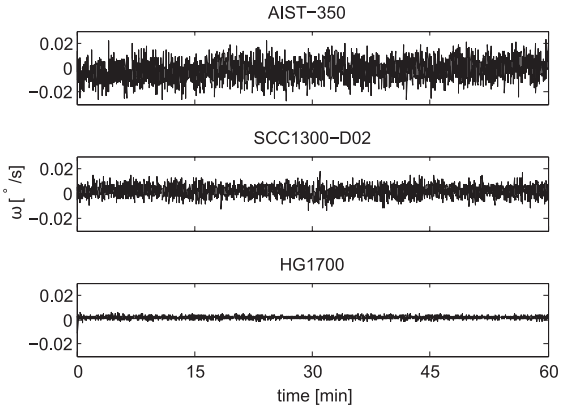

(*a*) Raw data.

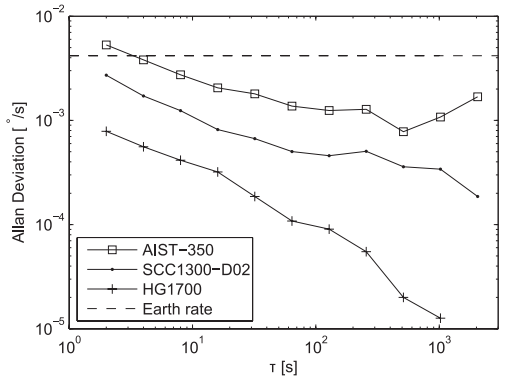

(*b*) Allan deviation.

Figure 1. Raw gyroscope data and the corresponding Allan deviation curves for three different sensors.

2. Theoretical background

According to the World Geodetic System 1984 (WGS84) model, the magnitude of the Earth's rotation rate is $\Omega_e = 7292\,115 \times 10^{-11}$ rad s$^{-1} \approx 4.178 \times 10^{-3}$ deg s^{-1} [10]. Since the input range of a typical MEMS gyroscope is approximately ± 100 deg s^{-1}, it is clear that measuring the Earth's rotation using such equipment requires a careful error analysis and filter design. Scale factor errors, typically in the order of 1–2% and possibly asymmetric, do not have a significant effect with such weak signals, and temperature effects can be mitigated by keeping the unit at a constant temperature and allowing it to warm up prior to the tests. In this paper, we will concentrate on the most significant error sources, i.e. angular rate random walk, in-run bias instability and the temperature-dependent bias. A good measure to characterize the first two errors is the Allan variance, which is described in the following section.

2.1. Allan variance

Named after Dr David W Allan, the Allan variance is a measure for characterizing noise and stability in clock systems [11]. It analyzes a sequence of observations and estimates the intrinsic frequency noise of the system as a function of averaging time. Although the method was originally developed for clocks, it can easily be adapted for different types of data.

The computation of Allan variance starts by taking a long sequence of data and dividing it into disjoint bins based on averaging time τ. The equation for the Allan variance is as follows:

$$AVAR(\tau) = \frac{1}{2(n-1)} \sum_{i=1}^{n-1} [y(\tau)_{i+1} - y(\tau)_i]^2, \qquad (1)$$

where $AVAR(\tau)$ is the Allan variance as a function of the averaging time, y_i is the average value of the measurements in the bin i and n is the total number of bins. Analogously to statistical terminology, the square root of Allan variance is known as the Allan deviation.

Figure 1 shows three sets of gyroscope data and their Allan deviation plots; the relation between precision and Allan deviation is easy to see. For short averaging times, the Allan deviation is dominated by uncorrelated noise in the sensor output; in fact, the power of white noise is directly related to the value of the Allan deviation at small τ [12]. Initially, the Allan deviation decreases as the averaging time gets longer. Then, at some point, the Allan deviation levels off because of $1/f$ noise [13], and eventually, with long averaging times,

it starts to increase. This is due to bias drift or rate random walk error in the sensor output, a process which is clearly non-stationary[1] [12]. The power of $1/f$ noise is commonly used to define bias instability [14] and thus, the minimum value of the Allan variance can be used as a measure of bias instability.

Allan variance is a very useful tool in the error analysis of MEMS-based navigation where the $1/f$ noise and random walk components are typically very strong. For example, consider a problem where the gyroscope bias needs to be estimated from the output of a stationary gyroscope. If the sensitivity axis of the gyroscope is aligned with the east–west direction, it is known that the actual input is zero. To estimate the bias, one can then obtain a sequence of measurements and take the average; the minimum point of the sensor's Allan variance plot indicates the best choice of averaging time. When the gyroscope output is used to compute the attitude, the estimated bias is subtracted from the measurements and the difference is integrated (i.e. summed as the measurements are discrete) to obtain the change in orientation over time. The estimate of the bias obtained as described above is not necessarily optimal, as the error process is correlated in time [15], but suffices for our purpose.

2.2. Modeling the gyroscope measurement

In this study, the aim is to observe the horizontal component of the Earth's rotation rate in order to find the true north orientation using a single gyroscope sensor aligned parallel to the local level. The output of the gyroscope is an angular rate measurement which we will model as

$$\omega^{+}(\varphi, \psi) = \Omega_e \cos\varphi \cos\psi + b \tag{2a}$$

$$\omega^{-}(\varphi, \psi) = -\Omega_e \cos\varphi \cos\psi + b, \tag{2b}$$

where b is the gyroscope bias and φ is the latitude. The observable component of the Earth's rate depends on the latitude because of the horizontal alignment of the sensor and on the angle ψ between the sensing axis and north direction. For example, when the sensing axis is parallel to the east–west direction ($\psi = \pm 90^\circ$), the Earth's rotation is not sensed at all.

Model (2*b*) is obtained by rotating the measurement setup by 180° and knowing that $\cos(\psi + 180^\circ) = -\cos\psi$. The motivation for the rotation is to be able to cancel the gyroscope bias: for each measurement orientation ψ, the magnitude of the Earth's rotation rate Ω_e can be estimated using (2*a*) and (2*b*) as follows:

$$\Delta\omega(\varphi, \psi) = \frac{\omega^{+}(\varphi, \psi) - \omega^{-}(\varphi, \psi)}{2} = \Omega_e \cos\varphi \cos\psi + \delta b, \tag{3}$$

where the term δb has been introduced to denote the possible change in the gyroscope bias b: since the opposite angular rate measurements (2*a*) and (2*b*) cannot be made simultaneously, the gyroscope bias b may have fluctuated between the measurements. In particular, the biases of MEMS gyroscopes are sensitive to temperature changes [16].

It is noteworthy that since the sensing axis of the gyroscope is perpendicular to the gravitational acceleration vector g in both (2*a*) and (2*b*), the components of g at the sensing and drive axes of a vibratory gyroscope remain unchanged when rotating the gyroscope from model (2*a*) to (2*b*) [2], and therefore the g-sensitivity effect is eliminated in difference (3). This is advantageous as the impact of the g-sensitivity on the measurements of a MEMS gyroscope can be significant [5].

As discussed in section 2.1, the noise process of a MEMS gyroscope is complicated. It has a $1/f$ component and another part of it is uncorrelated (white). However, modeling the $1/f$ noise component is tricky and can lead to complex fractional-order state models [17]; therefore, we approximate the noise process as a combination of white Gaussian noise and random walk. The random walk component is modeled in the unknown δb.

2.3. Estimating the north direction

Given the latitude φ and the Earth's rate Ω_e, the offset angle ψ can be estimated from (3). In this paper, an EKF is used to estimate the offset angle ψ from a sequence of such measurements with known shifts in ψ between the observations. The filter estimates a bivariate state vector

$$x_k = \begin{bmatrix} \psi_k \\ \delta b_k \end{bmatrix} \tag{4}$$

corresponding to the unknown quantities in (3) and k denoting the time. The offset angle ψ is modeled as piecewise constant with deterministic changes due to intentional rotations of the gyroscope setup, while δb is modeled as random walk plus linear correlation with the ambient temperature. The state propagation is modeled in discrete time as

$$x_k = x_{k-1} + \begin{bmatrix} \gamma_k \\ 0 \end{bmatrix} + q_k, \tag{5}$$

where γ_k denotes the gyroscope orientation change between the measurements $(k-1)$ and k, and q_k is a zero-mean Gaussian random vector with known covariance.

For updating the filter, we assume that temperature information is available along with the gyroscope output. We take the differenced angular rate (3) and the average sensor temperature difference between the measurements as the observations, yielding the Jacobian matrix

$$H = \begin{bmatrix} -\Omega_e \cos\varphi \sin\psi & 1 \\ 0 & \theta \end{bmatrix}, \tag{6}$$

where θ is the temperature coefficient of the gyroscope bias. In this study, the value of θ was determined empirically. Given initial conditions and the state propagation and measurement noise covariances, we can now construct an EKF [18].

It should be noted that the offset angle obtained using (2*a*) and (2*b*) is ambiguous: these equations do not give information about the sign of the angle ψ. Thus, the quadrant of ψ must be resolved when the initial state vector x_0 and its covariance are determined for the EKF. This can be done, e.g., by rotating the sensor 360° at a certain spacing and fitting a

[1] In contrast, the increments in random walk are stationary.

sine curve with known frequency but unknown phase to the measurements. However, this approach needs a considerable number of samples in order to work accurately enough, which means that it requires a long time to determine the initial state.

2.4. Error analysis

As long as the quadrant is known, the orientation of the gyroscope can be resolved from (3) as

$$\widehat{\psi} = \arccos \frac{\Delta\omega(\varphi, \psi)}{\Omega_e \cos\varphi} = \arccos\left(\cos\psi + \frac{\epsilon}{\Omega_e \cos\varphi}\right), \quad (7)$$

where $\widehat{\psi}$ denotes the heading estimate and ϵ is the uncompensated measurement error caused by gyroscope bias instability and noise. Computing the first-order Taylor series of this function enables estimating the effect of angular rate measurement errors on the computed orientation:

$$\widehat{\psi} \approx \psi - \frac{\epsilon}{\Omega_e \cos\varphi\sqrt{1-\cos^2\psi}}. \quad (8)$$

This result is in accordance with traditional gyrocompassing equations [2]. According to (8), the heading error due to uncompensated measurement errors is at its smallest when the sensor is in an east–west orientation (i.e. $\cos\psi = 0$), and the error is amplified as the sensor approaches the north–south direction.

When filtering the heading using the EKF, the precision of the orientation estimate improves with time, until it reaches a steady state. Given the variance of ϵ (essentially, the gyroscope bias instability) and the precision of the rotary stage movements, it is possible to estimate the attainable heading variance. Since the steady-state covariance matrix is not changed after taking a new filtering step, we have [18]

$$P = (I - KH)(P + Q) \quad (9a)$$

$$K = (P + Q)H^T\left(H(P + Q)H^T + R\right)^{-1}, \quad (9b)$$

where the time step indices k have been omitted, assuming that the state transition and measurement uncertainty covariances Q and R, respectively, are constant in time. Substituting (9*b*) into (9*a*) yields the discrete algebraic Riccati equation

$$Q - (P+Q)H^T(H(P+Q)H^T + R)^{-1}H(P+Q) = 0, \quad (10)$$

which can be solved for the steady-state covariance P. It should be noted that the Jacobian H changes depending on the current heading estimate; therefore, we can use the Jacobian of the optimal situation $\psi = 90^\circ$ to compute the lowest attainable estimate covariance. It is also possible to predict the lowest attainable covariance after n filter steps using the traditional EKF covariance propagation equations.

If the heading resolution algorithm were to be implemented as a batch least-squares solution instead of filtering, one would first collect a set of n measurements $\Delta\omega(\varphi, \psi_i + \psi)$ with $i = 1, \ldots, n$ and known ψ_i, and then use, e.g., the Gauss–Newton least-squares method to resolve the sensor orientation ψ. Assuming independent and identically distributed measurement errors with variance σ^2, the variance of the resulting heading estimate $\widehat{\psi}$ would be approximately equal to $\sigma^2(J^TJ)^{-1}$ with J representing the Jacobian of the system of equations:

$$J = -\Omega_e \cos\varphi[\,\sin(\psi_1 + \widehat{\psi}) \cdots \sin(\psi_n + \widehat{\psi})\,]^T. \quad (11)$$

Consequently, the variance of the heading estimate can be calculated as

$$\operatorname{var}\widehat{\psi} \approx \sigma^2\left(\Omega_e^2\cos^2\varphi\sum_{i=1}^{n}\sin^2(\psi_i + \widehat{\psi})\right)^{-1}, \quad (12)$$

which is minimized when all the squared sine terms equal 1, i.e. if all the observations were made with the input axis pointing to the east or west. An advantage of the least-squares method would be that it does not require knowledge of the distribution of the initial state. On the other hand, the EKF natively adopts to the state propagation model (5): for example, it accounts for the random walk error caused by the imprecision of the rotary stage movements by increasing the variance of the heading estimate accordingly after each rotation.

Table 1. The gyroscopes appearing in figure 1.

Model	Technology	Grade	Reference
AIST-350	MEMS, oven-conditioned	Mobile devices	[19]
SCC1300-D02	MEMS	Automotive	[20]
HG1700	Ring laser	Tactical	[21]

3. Hardware implementation

In this section, the gyrocompassing system proposed in this paper is presented. Since the key component of a gyrocompassing system is, of course, the gyroscope, we first discuss the choice of this sensor. Then, other necessary components and the structure of the system are presented.

3.1. Choosing the gyroscope

As discussed in section 2.1, bias instability is a major source of errors in the output data of a gyroscope sensor. For gyrocompassing applications, the bias instability of the gyroscope must be significantly lower than the Earth's rate. Figure 1(*b*) presents the Allan deviations of three gyroscopes based on different technologies; these sensors are described in table 1. From the figure it can be seen that the bias instability of each of the three sensors lies well below the Earth's rate (dashed line). However, relation (3) between the latitude, the orientation of the sensor and the observable Earth's rate should be borne in mind; for instance, this study was conducted in an area where only half of the Earth's rate is observable for a leveled gyroscope. Nevertheless, at an averaging time $\tau = 1000$ s, the Allan deviation of the SCC1300-D02 sensor is approximately 0.000 34 deg s^{-1} which is less than one-tenth of the theoretical Earth rate. Obviously, the closer to the poles

Table 2. SCC1300-D02 gyroscope sensor specifications [20].

Parameter	Value (deg s^{-1})
Operating range	± 100
Noise (RMS)	0.06
Short term instability	<0.0003
Quantization	0.05

Table 3. Components of the measurement setup.

Component	Description
Gyroscope	VTI SCC1300-D02 sensor [20]
USB/SPI interface	National Instruments NI USB-8451 device [23]
Power supply	Hewlett–Packard E3611A dc power supply, 0–20 V and 1.5 A
Regulator	Self-manufactured voltage regulator, 5 Vdc and 3.3 Vdc
Laptop	For reading (and saving) data and for controlling the rotary stage
Rotary stage	Velmex B5990TS rotary stage for changing the orientation of the gyroscope
Driver	For controlling the motor of the rotary stage

one goes in latitude, the better bias instability is required [2]; in the extreme case of $\varphi = \pm 90^\circ$, there is no horizontal Earth's rotation component and a north direction does not even exist.

According to figure 1, the ring laser gyroscope is clearly the best, which is not surprising. When comparing the two MEMS sensors, the SCC1300-D02 is better suited for gyrocompassing than the temperature-stabilized AIST-350 gyroscope because of the lower Allan variance; thus, we choose to use the VTI SCC1300-D02 in the gyrocompassing system. The most important performance values for this gyroscope are listed in table 2. It can be seen that the quantization of the sensor output is coarser than the Earth's rate. However, the gyroscope noise will cause stochastic dithering of the measurement prior to the analog-to-digital conversion, and thus it should be possible to estimate the Earth's rate given a sufficient number of samples [22].

3.2. Gyrocompassing system

The most essential hardware components of the measurement setup are described in table 3. In addition, for including the SCC1300-D02 sensor in the setup, a custom-printed circuit board was designed. In principle, the system is operated by a laptop computer which first reads data from the gyroscope, and then commands the rotary stage to rotate the sensor. A block diagram depicting the connections between the system's main components in more detail is presented in figure 2, and the entire measurement system is illustrated in figure 3.

For processing the data and also for controlling the rotary stage, we used MATLAB R2008a software. Furthermore, in order to collect and save the data from the SCC1300-D02 sensor, a software application was developed in Microsoft Visual Studio 2008. This application uses the NI USB-8451 device as a hardware interface between the sensor and the laptop. The maximum sampling rate attained for reading the

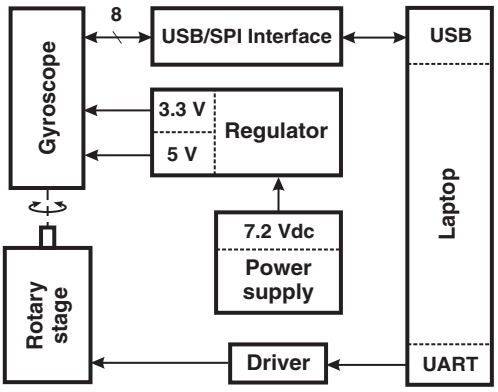

Figure 2. Block diagram showing the connections between the main components.

gyroscope output was approximately 1 kHz; this value was limited by the NI USB-8451 SPI interface.

In addition, the temperature of the gyroscope was measured at a sampling frequency of 2 Hz using the internal temperature sensor of the SCC1300-D02 gyroscope. The performance figures of the temperature sensor are not given in the gyroscope's specification sheet, but experiments have shown that the standard deviation of the short-term temperature measurement noise is in the order of 0.1 °C in the test environment; the sensor temperature varied between 25 and 28 °C during an observation period of 4 h.

4. Experimental results and discussions

In the previous section, a measurement setup was proposed, and it was shown that its specifications meet the theoretical requirements of gyrocompassing. In this section, we demonstrate that the setup is capable of gyrocompassing in practice. First, we show that the gyroscope is precise enough to observe the Earth's rotation; then, we evaluate its performance in the inverse problem, i.e. estimation of the orientation of the sensor given the Earth's rotation rate. All the measurements presented in this section were conducted in an office environment in Tampere, Finland, at latitude $\varphi \approx 61.449^\circ$N.

4.1. Measuring the Earth's rotation

In order to implement a gyrocompassing system, the gyroscope must be able to measure the rotation of the Earth to a sufficient accuracy. This capability can be verified in an experiment where the gyroscope is set sequentially into four different orientations—namely the principal compass points–and the output is logged at each position for a certain time. Then, since the offset angles ψ are known, the magnitude of the Earth's rate can be estimated.

The experiment was carried out such that the sensor stayed at each orientation for 5 min and was then automatically rotated 90° clockwise to the next measurement position. This process was continued for several hours. The sensing axis remained

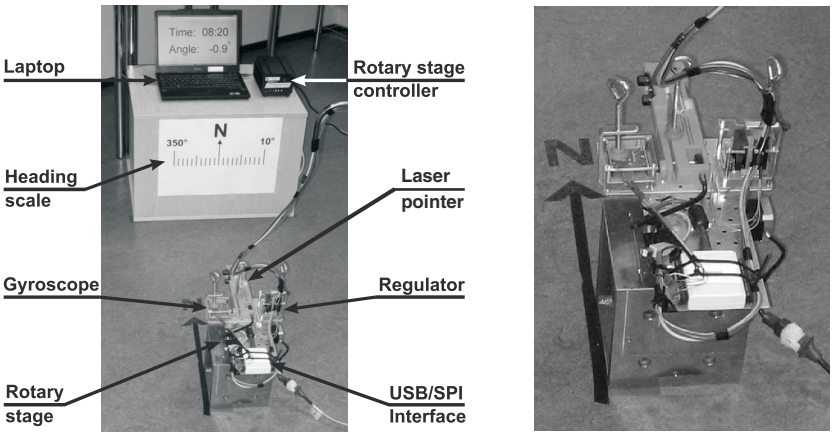

(*a*) Entire setup (*b*) Sensor and rotary stage

Figure 3. Measurement setup.

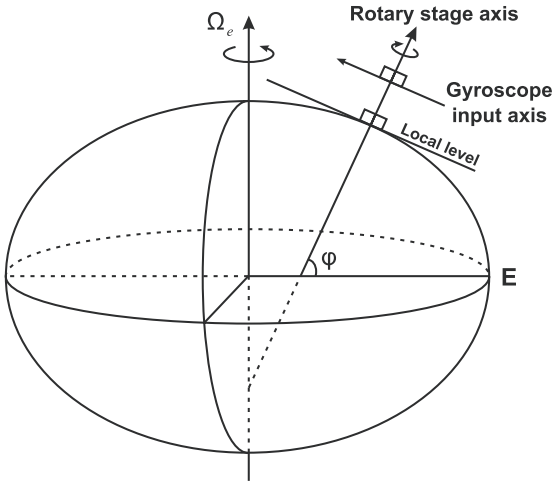

Figure 4. The sensitive axis of the gyroscope stays perpendicular to the local vertical while the rotary stage is turning.

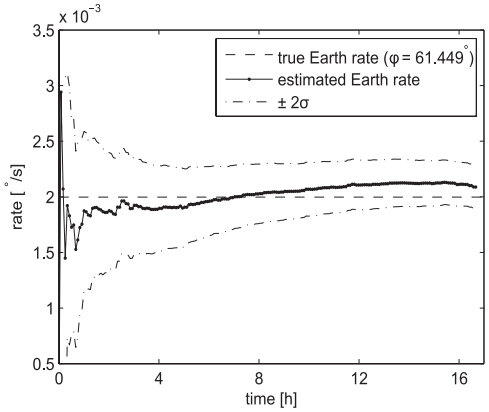

Figure 5. Earth rate estimation results.

parallel to the local level, as depicted in figure 4, for the entire time. Finally, the collected data were post-processed using a Kalman filter [5]. The underlying models used in the filter are basically similar to the equations presented in section 2.2, but the unknowns, i.e. the state vectors, are different, hence the measurement matrices are too.

The resulting estimates of the Earth's rate are presented in figure 5. Despite the fact that less than half ($\cos 61^\circ < 0.5$) of the Earth's rotation could be sensed by the gyroscope due to its horizontal alignment, the Earth's rate was still observed without difficulty. As can be seen from figure 5, the estimated Earth's rotation is very close to the theoretical value; after 16 h of measurements, the 2σ deviation of the estimate is 0.1932×10^{-3} deg s^{-1}, which is approx. 10% of the theoretical observable value 1.997×10^{-3} deg s^{-1}. Arnaudov and Angelov [4] achieved an estimation error of 8.7 %, but it should be noted that they were measuring the full Earth's rate, i.e. not only its horizontal component, which is approximately twice as large as our theoretical reference. Furthermore, figure 5 shows that the 2σ interval is overestimating the actual error; hence, it can be concluded that given a long measurement time, the proposed setup can measure the Earth's rate relatively well.

4.2. Gyrocompassing results

Since the SCC1300-D02 gyroscope was observed to be capable of measuring the Earth's rotation, a gyrocompassing system was constructed using the EKF described in section 2.3. This system is similar to the system used for estimating the Earth's rate; however, now the sensor is not rotated in a deterministic way (i.e. in 90° steps) but based on the measured Earth's rate.

Although the word 'gyrocompassing' usually refers to seeking the north direction, it is not obvious that it would be the easiest direction to find. In fact, when the offset angle ψ is zero, the Jacobian matrix (6) becomes singular and the covariance estimate sequence fails to converge; the Riccati equation (10) has no solution in that case. Figure 6 shows

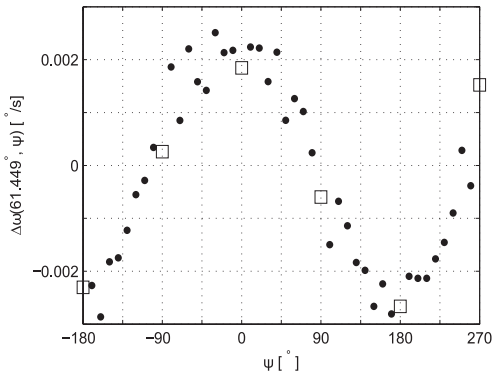

Figure 6. Differenced angular rates (3) from a 450° rotation spaced by 10°. Observations made at the principal compass points are denoted by squares.

the differenced measurements (3) from a rotation of 450° spaced by 10° with $\omega^+(\varphi, \psi)$ and $\omega^-(\varphi, \psi)$ both averaged for 5 min at each position. It can be seen that the slope of the measurements is at its steepest in the east–west direction; this is in accordance with the observation based on (8) that heading errors are minimized in this orientation. Hence, the system was tuned to seek east instead of north—obviously, it is trivial to find north given the east direction.

The EKF was used as a control loop for the Velmex rotary stage. The algorithm consists of two steps. First, the magnitude of the Earth's rotation rate was measured according to (3). Then, the measurement was fed to the EKF and the resulting state estimate was used to rotate the gyroscope's sensitivity axis toward east. Finally, the state estimate was propagated according to (5) with γ_k equal to the rotation. This procedure was repeated for several hours. As discussed in section 2.4, this approach yields the minimal variance because it aligns the input axis of the gyroscope with the east–west direction.

Figure 7 shows the gyrocompassing results for two separate measurement runs. In both cases, the system was initially offset from the true east direction by 90°, and at each position, the gyroscope output was averaged 5 min for ω^+ and another 5 min for ω^-. The results show that the system reached the true east orientation after 2 h, but the convergence of the covariance estimate takes more time. In fact, the covariance matrix did not reach a steady state in 8 h, but it can be seen that the 2σ confidence intervals get narrower as time passes.

After 2 h in both the tests shown in figure 7, the true east direction stays within the 2σ bounds corresponding to the EKF covariance estimate, although at the end of case 7(a), the true value is fairly close to the boundary. Initially, the true orientation (zero error line) does not lie between the 2σ lines, which is due to too optimistic an initial covariance estimate. Nevertheless, the accuracy of the system was in both cases better than 5° in terms of both absolute accuracy and the 2σ bounds; the final 2σ deviation was 4.03° in both runs. In autonomous dead reckoning, a heading error of 5° would cause a cross-track error of around 9 m after 100 m of navigation; obviously, this accuracy is inadequate for long-term autonomous navigation. Furthermore, an initialization

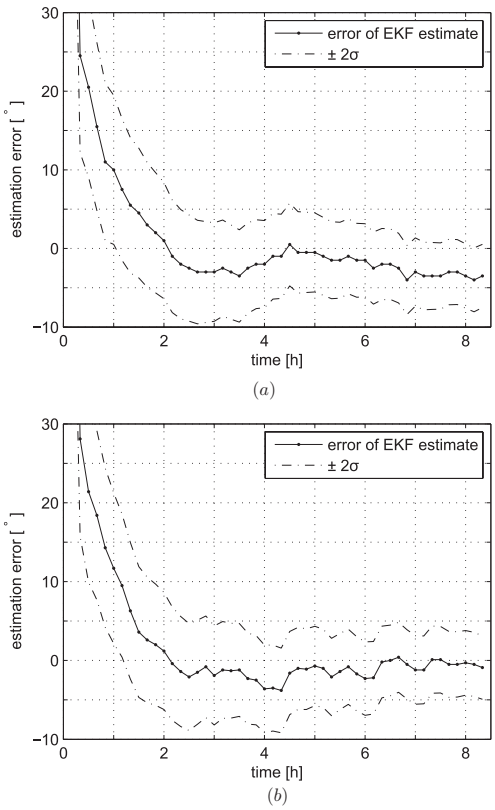

Figure 7. Gyrocompassing results obtained in two runs. The initial offset angle was 90° from the east direction in both cases; the first estimates have been cropped out.

time of 8 h would be infeasible for most applications. However, in light of these results it is clear that gyrocompassing is possible using a low-cost MEMS gyroscope and a simple rotary stage even at relatively high latitudes.

5. Conclusions

In this paper, a gyrocompassing system based on a single low-cost VTI SCC1300-D02 MEMS gyroscope sensor was presented. The most significant error sources that deteriorate MEMS gyroscope measurements were compensated for by keeping the sensor aligned with the horizontal plane, by rotating it according to a certain sequence, and by error estimation using an EKF. This enabled observing very small angular rates, such as the Earth's rotation rate.

Since the tests were conducted in an office environment, rapid temperature fluctuations did not occur. Therefore, temperature compensation based on the measured sensor temperature and a temperature coefficient θ was regarded as sufficient along with the bias compensation based on mechanical rotations. The temperature of the gyroscope can change rapidly during the initial warm-up phase, but

this was not observed to have caused any problems in the experiments.

The mechanical structure of the experimental setup was fairly simple, consisting mainly of a leveled rotary stage with a gyroscope mounted on it, and a controller to control the stage. Thus, all necessary rotations were made around one single axis, avoiding the need for complex mechanics and gimbals. The horizontal orientation of the rotary stage could be verified, e.g., using accelerometers [2]; the SCC1300-D02 does include a three-axis accelerometer in addition to the gyroscope, but leveling is beyond the scope of this paper.

In the paper, it was shown that the SCC1300-D02 gyroscope is accurate enough to measure the Earth's rotation. The results show that with the implemented EKF-based control loop, two-sigma accuracies of approximately 4° were attained. A drawback of aligning the sensor parallel to the local level is that a fraction of the observable Earth's rate is lost, but it was proven that the proposed system can still work at a latitude of 61°. Anyway, the performance of the proposed system depends on the latitude.

As future work, more sophisticated initialization algorithms to obtain the initial state for the EKF and to resolve the sign ambiguity should be developed. In the initialization phase, the sinusoidal regression approach mentioned in this paper requires many samples in order to work reliably. The proposed setup needs hours of time to reach a five-degree-level accuracy, which is infeasible for real-life applications. However, in the future, as the MEMS gyroscope technology progresses, shorter and shorter averaging times can be used, enabling faster north seeking. In conclusion, the results obtained in this study demonstrate the accuracy potential that can be attained using a low-cost, thumbnail-size sensor with small power consumption.

References

[1] Honeywell International Inc. 2006 Data sheet for Honeywell μPoint HMR3600 digital magnetic compass

[2] Titterton D H and Weston J L 2004 *Strapdown Inertial Navigation Technology* 2nd edn (Reston, VA: AIAA)

[3] Iozan L I, Kirkko-Jaakkola M, Collin J, Takala J and Rusu C 2010 North finding system using a MEMS gyroscope *Proc. European Navigation Conf. on Global Navigation Satellite Systems (Braunschweig, Germany)*

[4] Arnaudov R and Angelov Y 2005 Earth rotation measurement with micromechanical yaw-rate gyro *Meas. Sci. Technol.* **16** 2300–6

[5] Iozan L I, Collin J, Pekkalin O, Hautamäki J, Takala J and Rusu C 2010 Measuring the Earth's rotation rate using a low-cost MEMS gyroscope *Proc. 2010 Symp. Gyro Technology (Karlsruhe, Germany)* pp 20.1–20.16

[6] Barbour N and Schmidt G 2001 Inertial sensor technology trends *IEEE Sensors J.* **1** 332–9

[7] Lapadatu D, Blixhavn B, Holm R and Kvisteroy T 2010 SAR500—A high-precision high-stability butterfly gyroscope with north seeking capability *Position Location and Navigation Symp. (PLANS) (Palm Springs, CA)* pp 6–13

[8] Johnson B R, Cabuz E, French H B and Supino R 2010 Development of a MEMS gyroscope for northfinding applications *Position Location and Navigation Symp. (PLANS) (Palm Springs, CA)* pp 168–70

[9] Renkoski B M 2008 The effect of carouseling on MEMS IMU performance for gyrocompassing applications *SM Thesis* Massachusetts Institute of Technology, MA

[10] 2000 Department of Defense World Geodetic System 1984: Its definition and relationships with local geodetic systems National Imagery and Mapping Agency *Technical Report* TR8350.2

[11] Allan D W 1966 Statistics of atomic frequency standards *Proc. IEEE* **54** 221–30

[12] IEEE standard specification format guide and test procedure for single-axis laser gyros 1996 *IEEE Std 647-1995*

[13] Voss R F 1979 $1/f$ (flicker) noise: A brief review *Proc. 33rd Annu. Symp. Frequency Control* pp 40–6

[14] IEEE Standard for Inertial Sensor Terminology 2001 *IEEE Std 528-2001*

[15] Beran J 1994 *Statistics for Long-Memory Processes* (London/Boca Raton, FL: Chapman and Hall/CRC Press)

[16] El-Diasty M, El-Rabbany A and Pagiatakis S 2007 Temperature variation effects on stochastic characteristics for low-cost MEMS-based inertial sensor error *Meas. Sci. Technol.* **18** 3321–8

[17] Sierociuk D and Dzielinski A 2006 Fractional Kalman filter algorithm for the states, parameters and order of fractional system estimation *Int. J. Appl. Math. Comput. Sci.* **16** 129–40

[18] Grewal M S and Andrews A P 1993 *Kalman Filtering: Theory and Practice* (Englewood Cliffs, NJ: Prentice-Hall)

[19] iSense LLC 2010 Data sheet for MEMS IMU AIST-350

[20] VTI Technologies 2010 SCC1300-D02 combined gyroscope and 3-axis accelerometer with digital SPI interfaces

[21] Honeywell International Inc. 2010 Data sheet for Honeywell HG1700 IMU

[22] Aumala O 1996 Turning interference and noise into improved resolution *Measurement* **19** 41–8

[23] National Instruments 2007 NI USB-8451 data sheet